J. Fluid Mech. (1968), *vol.* 31, *part* 1, *pp.* 95–112
Printed in Great Britain

On the flow between a rotating and a stationary disk

By G. L. MELLOR, P. J. CHAPPLE† AND V. K. STOKES‡
Department of Aerospace and Mechanical Sciences, Princeton University

(Received 28 April 1967)

The analysis and experiments in this paper are restricted to the flow between two coaxial, infinite disks, one rotating and one stationary. The results of numerical calculations show that many solutions can exist for a given Reynolds number $\Omega l^2/\nu$ (Ω is the angular velocity of the rotating disk and l is the spacing between the two disks). Out of a greater number of possible solutions, three solution branches have been identified; the branches correspond to one-, two- and three-flow cells in the meridional plane.

The one-cell branch has been accorded detailed treatment. Within this branch there are two subbranches. The first, now well documented in the literature, includes solutions from zero to infinite Reynolds number. The latter limiting case is characterized by an inward-flowing boundary layer on the stationary disk and an outward-flowing boundary layer on the rotating disk. In between is a core flow rotating with a constant angular velocity. The second sub-branch of the single-cell flows, apparently unknown heretofore, begins with an infinite Reynolds number, decreases to a minimum and then increases to an infinite Reynolds number again. The first infinite Reynolds number limit again corresponds to two boundary-layer flows separated by a core flow with constant angular velocity opposite in direction to the angular velocity of the rotating disk. The second limiting case of infinite Reynolds number is the free-disk solution of von Kármán (1921). Asymptotic solutions have been obtained which more fully describe the nature of this flow as the Reynolds number increases.

The second part of the paper presents experimental measurements corresponding to the Reynolds number range 0–100. Profiles were measured with a hot-wire anemometer. The measurements are in agreement with the first, one-cell branch of solutions. A semi-quantitative evaluation of edge effects is obtained.

1. Introduction

Discussion of the steady flow of a viscous incompressible fluid between two infinite disks is often generalized to cases where the ratio of their angular velocities is arbitrary. However, in this paper we restrict discussion to cases where one disk is stationary. Reynolds number is then the only apparent independent variable.

The problem has aroused interest because of the possibility of obtaining exact solutions to the Navier–Stokes equations for any Reynolds number;

† Bristol-Siddeley Engines Ltd., P.O. Box 3, Filton, Bristol, England.
‡ Indian Institute of Technology, Kanpur, India.

as the Reynolds number increases one would expect to observe the evolution of a boundary layer and a reasonable guess might be that the flow would approach the free-disk solution of von Kármán (1921) such that, outside of the rotating-disk boundary layer, the radial and tangential velocities would tend to zero. However, Batchelor (1951), in an early extension of von Kármán's formulation, argued that the main body of fluid would rotate with constant angular velocity and boundary layers would develop on *both* disks as the Reynolds number increased. This view was later challenged by Stewartson (1953), who argued that the free-disk solution of von Kármán was, in fact, the proper limiting case for large Reynolds number. He based his reasoning on the trend observed in solutions obtained with a series expansion for small Reynolds number. More recent numerical solutions by Lance & Rogers (1962) and by Pearson (1965) indicate clearly that the small Reynolds number trend is misleading and that Batchelor's qualitative picture of the flow was correct in all essentials.

The conclusion one might reach from the above evidence is that the free-disk solution of von Kármán is not a limiting case of the two-disk solutions. However, in the present paper the alternative result is demonstrated; the von Kármán solution is seen to be the limit solution of a certain branch of two-disk solutions as the Reynolds number increases. Furthermore, it is apparent that many other solutions for a single Reynolds number are possible.

The experimental results to be presented were obtained before the above picture was clear. The only data obtained correspond to the one-cell branch described by Batchelor, thus lending experimental verification to Batchelor's prediction.

2. The governing equations

The governing equations for an incompressible flow consist of the continuity equation and the three equations of motion. Assuming axial symmetry, they are

$$\frac{1}{r}\frac{\partial}{\partial r}(ru)+\frac{\partial w}{\partial z}=0, \tag{1}$$

$$u\frac{\partial u}{\partial r}+w\frac{\partial u}{\partial z}-\frac{v^2}{r}=-\frac{1}{\rho}\frac{\partial p}{\partial r}+\nu\left(\frac{\partial^2 u}{\partial r^2}+\frac{\partial}{\partial r}\left(\frac{u}{r}\right)+\frac{\partial^2 u}{\partial z^2}\right), \tag{2}$$

$$\frac{u}{r}\frac{\partial}{\partial r}(rv)+w\frac{\partial v}{\partial z}=\nu\left(\frac{\partial^2 v}{\partial r^2}+\frac{\partial}{\partial r}\left(\frac{v}{r}\right)+\frac{\partial^2 v}{\partial z^2}\right), \tag{3}$$

$$u\frac{\partial w}{\partial r}+w\frac{\partial w}{\partial z}=-\frac{1}{\rho}\frac{\partial p}{\partial z}+\nu\left(\frac{\partial^2 w}{\partial r^2}+\frac{1}{r}\frac{\partial w}{\partial r}+\frac{\partial^2 w}{\partial z^2}\right). \tag{4}$$

If we let l be the disk spacing (see figure 1), $z=0$ be the stationary disk position, while $z=l$ is the rotating-disk position and Ω its angular velocity, then the boundary conditions are

$$u(r,0)=0, \quad u(r,l)=0, \tag{5a,b}$$

$$v(r,0)=0, \quad v(r,l)=\Omega r, \tag{5c,d}$$

$$w(r,0)=0, \quad w(r,l)=0. \tag{5e,f}$$

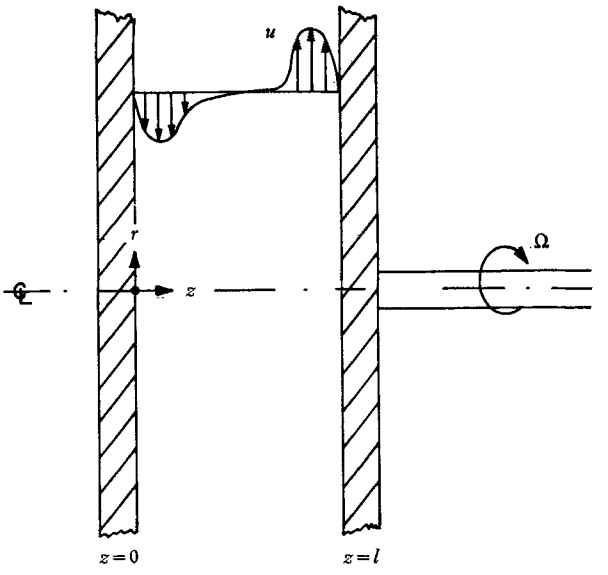

FIGURE 1. Sketch of the co-ordinate system. Except for the analysis in the appendix, the origin is located on the stationary disk.

Definitions	(*a*)	(*b*)	
	$z = l\xi$	$z = (\nu/\omega)^{\frac{1}{2}}\eta$	(6*a*, *b*)
	$v = \Omega r G(\xi)$	$v = \omega r g(\eta)$	(7*a*, *b*)
	$w = -2(\Omega l)\,H(\xi)$	$w = -2(\omega\nu)^{\frac{1}{2}}h(\eta)$	(8*a*, *b*)
	$u = \Omega r H'(\xi)$	$u = \omega r h'(\eta)$	(9*a*, *b*)
	$p/\rho = \Omega^2 l^2 \tilde{P}(\xi) + \frac{1}{2}\Lambda\Omega^2 r^2$	$p/\rho = \omega\nu\hat{P}(\eta) + \frac{1}{2}\lambda\omega^2 r^2$	(10*a*, *b*)
Equations			
	$(H'''/R) + 2HH'' - H'^2 = \Lambda - G^2$	$h''' + 2hh'' - h'^2 = \lambda - g^2$	(11*a*, *b*)
	$(G''/R) + 2HG' - 2H'G = 0$	$g'' + 2hg' - 2h'g = 0$	(12*a*, *b*)
	$\tilde{P}' = -2\{(H''/\mathrm{R}) + 2HH'\}$	$\hat{P}' = -2(h'' + 2hh')$	(13*a*, *b*)
Boundary conditions			
	$H(0) = 0$	$h(0) = 0$	(14*a*, *b*)
	$H(1) = 0$	$h(\eta_l) = 0$	(15*a*, *b*)
	$H'(0) = 0$	$h'(0) = 0$	(16*a*, *b*)
	$H'(1) = 0$	$h'(\eta_l) = 0$	(17*a*, *b*)
	$G(0) = 0$	$g(0) = 0$	(18*a*, *b*)
	$G(1) = 1$	$g(\eta_l) = 1$† or $g'(0) = 1$	(19*a*, *b*)

TABLE 1. The basic equations using different scaling factors. Note that equation set (*b*) is used in two ways depending on the definition of ω.†

† For $g(\eta_l) = 1$, set $\omega = \Omega$; for $g'(0) = 1$, set $\omega = \{(\nu^{\frac{1}{2}}/r)\,(\partial v/\partial z)_{z=0}\}^{\frac{2}{3}}$. Solutions in the form of set (*b*) may be rescaled in the form of set (*a*) by noting that $\Omega = \omega g(\eta_l)$ and $l = (\nu/\omega)^{\frac{1}{2}}\eta_l$.

In table 1, for reasons to be discussed, we have formed two sets of equations based on different dimensional schemes. Equations (6*a*)–(10*a*) or (6*b*)–(10*b*) are the assumed forms of the similarity solutions which result in the ordinary differential equations (11*a*)–(13*a*) or (11*b*)–(13*b*). The problem is to obtain solutions to the two simultaneous equations (11) and (12) after which (13) can be easily solved for the axial pressure variation. There are six boundary conditions for the fifth-order system of equations; however, the radial-pressure-gradient parameter, Λ or λ, is arbitrary and must also be determined.

In equation set (*a*) the Reynolds number, $R = \Omega l/\nu$, appears as a parameter in the differential equations. In equation set (*b*), if we set $\omega = \Omega$ (we shall later wish to change this definition), the Reynolds number appears as $\eta_l = R^{\frac{1}{2}}$. This latter set of equations is useful in the free-disk limit $R \to \infty$ whereas equation set (*a*) seems to be ideally suited to finite Reynolds numbers. For small R a series solution for small Reynolds number has been obtained by Stewartson (1953), Grohne (1955) and Lance & Rogers (1962). In our present nomenclature this can be written

$$G = \xi - \frac{R^2}{6300}(8\xi - 35\xi^4 + 63\xi^5 - 20\xi^7) + O(R^4), \tag{20a}$$

$$H = \frac{R}{60}(-2\xi^2 + 3\xi^3 - \xi^5) + O(R^3), \tag{20b}$$

$$\Lambda = \tfrac{3}{10} + O(R^2). \tag{20c}$$

3. Numerical solutions

Initially, our approach was to cast equations (11*a*) and (12*a*) in the form of integrals for $G(\xi)$ and $H(\xi)$. The integrals explicitly embraced the boundary conditions as their limits, but the integrands were functions of G, H and H', which were guessed. Numerical quadratures were obtained for improved solutions. We found that the iterations could be made to converge up to a Reynolds number of about 100, but beyond that nothing could be done to bring about convergence. All of this is described in detail in a report by Chapple & Stokes (1962).

Meanwhile, numerical solutions up to a Reynolds number of 441 appeared in the literature (Lance & Rogers 1962). These were obtained by the method of guessing Λ and two initial conditions over and above these provided at one disk and integrating the full equations to the second disk. An iteration proceeded until the three boundary conditions on the second disk were satisfied. Later Pearson (1965) applied the interesting method of solving the unsteady Navier–Stokes equations and obtaining the asymptotic steady solutions at large times. In particular he obtained a solution for a Reynolds number of 1000 which was an apparent continuation of the solutions of Lance & Rogers (1962) and left little doubt as to the asymptotic behaviour of the solutions for large Reynolds number. Batchelor's speculations were thus verified analytically.

In the interval 1962 to 1966 a revival of effort by the first author of this paper provided indication that the picture was not at all complete. After several trials the following procedure was adopted.

Equation set (b) forms the basis of our approach. The integration of (11b) and (12b) is started at the stationary disk, where we set $h(0) = h'(0) = g(0) = 0$. Furthermore, we define the free parameter, $\omega = \{(\nu^{\frac{1}{2}}/r)(\partial v/\partial z)_{z=0}\}^{\frac{2}{3}}$ so that $g'(0) = 1$. To start the integration we now need to specify only two parameters, $h''(0)$ and $h'''(0) = \lambda$.

For given values of $h''(0)$ and $h'''(0)$ the integration proceeds (we used a third-order Runge–Kutta technique) from $\eta = 0$ to some value where $g(\eta)$ exceeds some large number (we chose 10^6). In this interval, values of η where $h'(\eta) = 0$ were recorded along with the corresponding values of $h(\eta)$. For a given $h''(0)$,

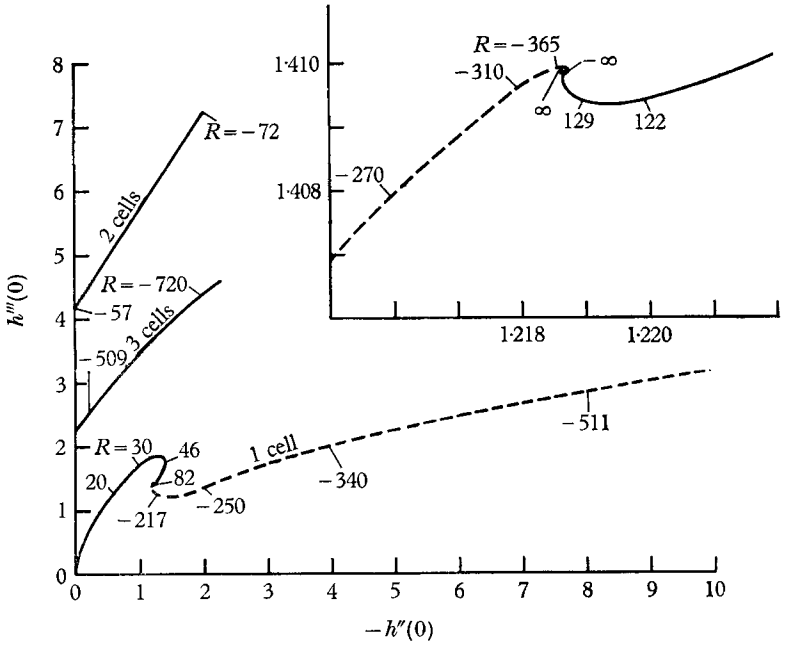

FIGURE 2. A map of the values $h''(0)$ and $h'''(0)$ which together with $h(0) = h'(0) = g(0) = 0$ and $g'(0)$ are the initial conditions to give any solution. The inset is a detail around the one-cell singular point seen in the main plot.

one could vary $h'''(0)$ until $h(\eta_l) = 0$ at the same η_l where $h'(\eta_l) = 0$. This would then constitute a solution to our problem, which, if desired, could then be rescaled to $G(\xi)$ and $H(\xi)$. (It is evident that $g(\eta_l) = \Omega/\omega$ and therefore $R \equiv \Omega l^2/\nu = \eta_l^2 g(\eta_l)$.)

With the above system at our disposal it is, in principle, possible to identify all possible solutions on a plot of $h'''(0)$ *vs.* $h''(0)$. In figure 2 we have only traced out a three-cell branch of solutions, a two-cell branch and *two* one-cell branches. A 'cell' is defined as the flow bounded by planes of constant z where $h = 0$ and therefore includes only its own recirculating fluid.

In figure 2 the first one-cell branch is shown as a solid line while the second one-cell branch is broken. At the juncture of these branches a very detailed treatment is required about a singular point where R approaches an infinite value. Where such points occurred in the two- and three-cell branches we have

	0·627	1·455	1·473	1·654	3·1	0·293	1·
	1·271	2·065	2·286	1·492	9·7	0·232	1·3
	1·702	2·440	3·234	2·653	19·2	0·163	2·0
	1·845	2·673	4·210	4·296	30·1	0·104	2·7
	1·782	2·938	5·392	6·687	46·5	0·0613	3·6
	1·589	3·302	6·210	8·610	67·9	0·0412	4·3
	1·433	4·005	6·039	8·360	96·9	0·0390	5·3
2	1·4102	4·798	5·042	6·350	116·1	0·0555	6·0
9	1·40944	5·487	4·284	4·852	129·0	0·0767	6·2
8715	1·40970	6·180	3·730	3·852	142·5	0·101	6·3
87561	1·40986	7·459	3·500	3·368	194·7	0·122	7·1
87687	1·409872	8·176	3·568	3·487	238·5	0·111	7·9
87710	1·4098732	8·553	3·636	3·605	265·9	0·107	8·4
87722	1·4098731	9·337	3·867	3·930	337·1	0·0943	9·4
87724	1·4098730	∞	3·837	3·954	∞	0·1018	∞
		∞	−10·04	−19·19	$-\infty$	0·0140	$-\infty$
87726	1·4098726	9·616	−10·36	−20·21	−957·8	0·0131	−18·7
87730	1·4098728	9·386	−10·19	−20·45	−897·9	0·0136	−18·8
87793	1·4098801	8·406	−10·01	−18·82	−707·3	0·0141	−15·8
872	1·409946	6·792	− 8·50	−14·96	−392·3	0·0145	−11·9
8	1·409621	5·902	− 8·880	−16·03	−309·4	0·0179	−10·6
	1·40079	4·825	−11·15	−22·77	−259·5	0·0126	−9·8
	1·2569	3·453	−18·20	−47·28	−217·0	0·0038	−8·9
	1·2389	3·222	−21·07	−58·89	−218·8	0·0028	−9·0
	1·3726	2·662	−35·38	−127·9	−250·6	0·0011	−9·6
	1·988	2·086	−80·66	−442·3	−350·9	0·0003	−11·4
	2·483	1·825	−131·3	−921·8	−437·5	0·0001	−12·8
	3·1576	1·548	−241·4	−2320·0	−578·6	—	−14·8
	4·1052	1·244	−519·4	−7308·0	−803·2	—	−17·5
	5·3600	0·937	−1321·0	−30520·0	−1162·0	—	−21·6
0	∞	0	∞	∞	∞	0	∞

2·2216	5·510	−16·32	−36·84	−494·5	0·0083	−12
2·4872	5·445	−17·25	−40·18	−511·4	0·0084	−12
3·0013	5·325	−19·29	−47·66	−547·1	0·0081	−13
3·4801	5·215	−21·62	−56·53	−588·0	0·0074	−13
3·901	5·102	−24·35	−67·61	−633·9	0·0066	−14
4·358	—	—	—	−720·0	—	
			Two-cell solutions			
4·162	6·945	−1·22	−3·183	−58·9	2·79	−18
5·070	6·767	−1·349	−3·695	−61·7	2·79	−18
5·695	6·693	−1·435	−4·046	−64·2	2·76	−18
6·310	6·631	−1·527	−4·422	−67·2	2·71	−19
7·235	6·582	−1·663	−4·993	−72·0	2·62	−19

TABLE 2. $h'''(0)$ and $h''(0)$ together with $h(0) = h'(0) = g(0)$ and $g'(0) = 1$ are the initial conditions. $\Lambda = h'''(0)/g(\eta_l)^2$ and $G'(1) = \eta_l g'(\eta_l)/g(\eta_l)$ are the rescaled radial pressure gradient and tangential velocity gradient on the rotating disk.

utions obtained by matching numerical solutions near the rotating and stationary disks with analytical solutions applicable t

von Kármán (1921) free-disk limit solution. Here, our calculations agree with those obtained by Cochran (1934).

discontinued the investigation. In the case of the one-cell solutions, a detail is shown for the neighbourhood of the singular point. In all but the first one-cell branch $g(\eta)$ changes sign and such solutions have been designated by negative values of R. However, this is merely a convention of the present paper since, if, for $R = R_1$, g_1 and h_1 are a solution, then, for $R = -R_1$, $g_2 = -g_1$ and $h_2 = h_1$ are another solution. Table 2 lists the numerical values of $h''(0)$ along with useful values at the rotating disk, e.g. $g'(\eta_i)$ or $G'(1)$, which can be used to compute the torque exerted by the fluid on the rotating disk.

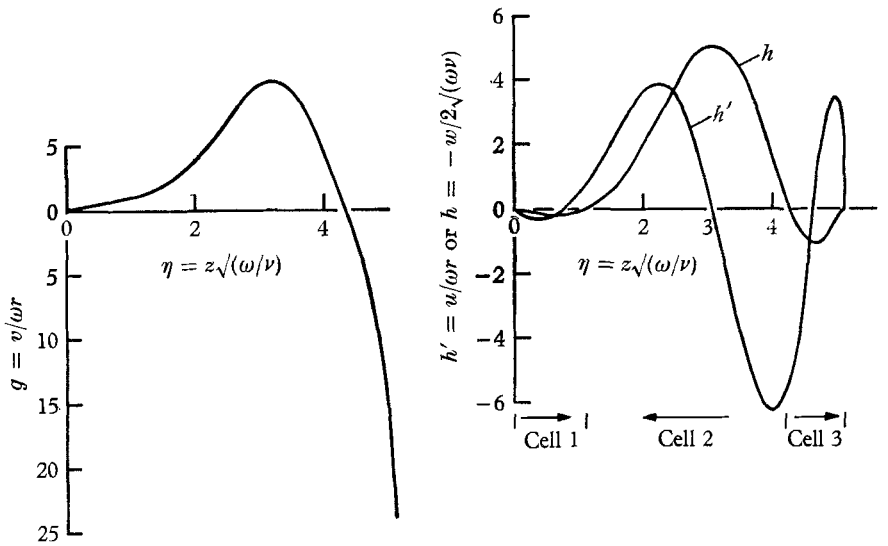

FIGURE 3. A sample multi-cell solution.

As noted previously we have carried out a detailed study of the two branches for only the one-cell cases. However, before discussing these solutions, sample three-cell solutions are illustrated in figure 3.

We believe, but cannot prove, that the one-cell solutions have been determined completely. The start of the sequence at $h''(0) = h'''(0)$ when $R = 0$ is given by equations (20a, b, c) in the form of $G(\xi)$ and $H(\xi)$. Then, using the numerical routine $h''(0)$ and $h'''(0)$ are varied as previously described so as to satisfy the outer boundary conditions. In table 2 it will be seen that, to reach the value $R = 337$ or $R = -958$, one must finally resort to variations of $h''(0)$ and $h'''(0)$ in the eighth decimal place, which is the limit of significance of the present calculation.† As seen in the solutions of figures 4 and 5, a solid-body rotational core develops between the stationary and rotating disks where $g(\eta) \simeq g_0 = \text{const.}$ and $h(\eta) \simeq h_0 = \text{const.}$

To investigate the solution as $R \to \pm\infty$, we must analyse the core flow in some detail. There, it should be possible to set

$$g(\eta) = g_0 + g_1(\eta), \quad h(\eta) = h_0 + h_1(\eta), \tag{21a, b}$$

† We used evenly spaced intervals of $\Delta\eta = 0{\cdot}01$. Halving the interval yielded no significant change in the results except to alter the required value $h''(0)$ for a given $h'''(0)$ in the seventh decimal place.

where g_1, h_1 and all their derivatives are assumed to be small. Substituting $(21a, b)$ into $(11b)$ and $(12b)$, setting $\frac{1}{2}\lambda = g_0^2$ and neglecting products of g_1, h_1 and their derivatives yields

$$h_1''' + 2h_0 h_1'' + 2g_0 g_1 = 0, \quad g_1'' + 2h_0 g' - 2g_0 h_1'' = 0. \tag{22,ab}$$

Solutions to $(22a, b)$ can be obtained in the form

$$g = g_0 + A_1 \exp\{\mathscr{R}_1 \eta\} \cos\{\mathscr{I}_1 \eta - \phi_1\} + A_2 \exp\{\mathscr{R}_2(\eta - \eta_0)\} \cos\{\mathscr{I}_2(\eta - \eta_0) - \phi_2\}, \tag{23a}$$

$$h' = A_1 \exp\{\mathscr{R}_1 \eta\} \sin\{\mathscr{I}_1 \eta - \phi_1\} + A_2 \exp\{\mathscr{R}_2(\eta - \eta_0)\} \{\sin\{\mathscr{I}_2(\eta - \eta_0) - \phi_2\}, \tag{23b}$$

where $\left.\begin{matrix}\mathscr{R}_1 \\ \mathscr{R}_2\end{matrix}\right\} = h_0\{-1 \pm (1+q^2)^{\frac{1}{2}} \cos\theta\}$, $\left.\begin{matrix}\mathscr{I}_1 \\ \mathscr{I}_2\end{matrix}\right\} = h_0\{\mp (1+q^2)^{\frac{1}{2}} \sin\theta\}$

and $q = 2g_0/h_0^2$, $\theta = \frac{1}{2}(\tan^{-1} q)$. A_1, ϕ_1, A_2, ϕ_2 are arbitrary constants. Since we shall find $\mathscr{R}_1$ to be negative and $\mathscr{R}_2$ positive, the additional constant η_0 has been introduced as a convenience by which the core size may be increased as the Reynolds number is increased.

The Bödewadt solution

The Bödewadt (1940) solution whereby the flow is asymptotic to zero radial velocity and solid-body rotational velocity as $\eta \to \infty$ may be obtained by setting $g_0 = 1{\cdot}183$, $h_0 = -0{\cdot}743$, $A_1 = 1{\cdot}2926$, $\phi_1 = 5{\cdot}991$ and $A_2 = 0$. These values are, of course, obtained by matching equations $(23a, b)$ to the numerical solution corresponding to $h''(0) = -1{\cdot}2187724$, $h'''(0) = 1{\cdot}4098730$. In fact, the two solutions match surprisingly well over the entire interval $3 < \eta < 7$.

The two one-cell solutions for $R \to \pm\infty$

Again, with $g_0 = 1{\cdot}183$ and $h_0 = -0{\cdot}743$ and with very large η, the procedure is to use equations $(23a, b)$ to determine initial values at $\eta = \eta_0$ for h, h', h''', g and g', which are used to restart the numerical calculation. For any small value of A_2 (since η_0 is arbitrary) a solution can then be determined for a given ϕ_2.

Two solutions were found in this manner which satisfy the outer boundary conditions. For $A_2 = 0{\cdot}001$ we found $\phi_2 = 2{\cdot}1677$ and $\phi_2 = 0{\cdot}2566$ at $\eta = \eta_0$.

In figures 4 and 5 the two solutions are shown and labelled $R = \pm\infty$. It should be noted that the numerical solutions and equations $(23a, b)$ match well so long as $\eta - \eta_l < -1{\cdot}5$.

An examination of figures 4 and 5 indicates that our solutions for $R = \pm\infty$ are indeed the limit solutions of the two one-cell branches and that, with the help of equations $(23a, b)$, flows for Reynolds numbers in the range

$$337 < R < \infty \quad \text{and} \quad -\infty < R < -958$$

may be obtained by varying η_0.

Approach to the von Kármán flow

In figure 5 (or see figure 2) the absolute Reynolds number goes through a minimum and then increases. At $R = -437$ the solutions are in need of re-scaling, and this is achieved by setting $\omega = \Omega$ (instead of that necessary to

give $g'(0) = 1$). Figure 6 continues plots of the solution in the rescaled (von Kármán 1921) co-ordinates. As will now be seen the flow approaches the free-disk solution as $R \to -\infty$, and a rather interesting and simple situation develops. The limiting behaviour can be obtained according to the 'method of matched

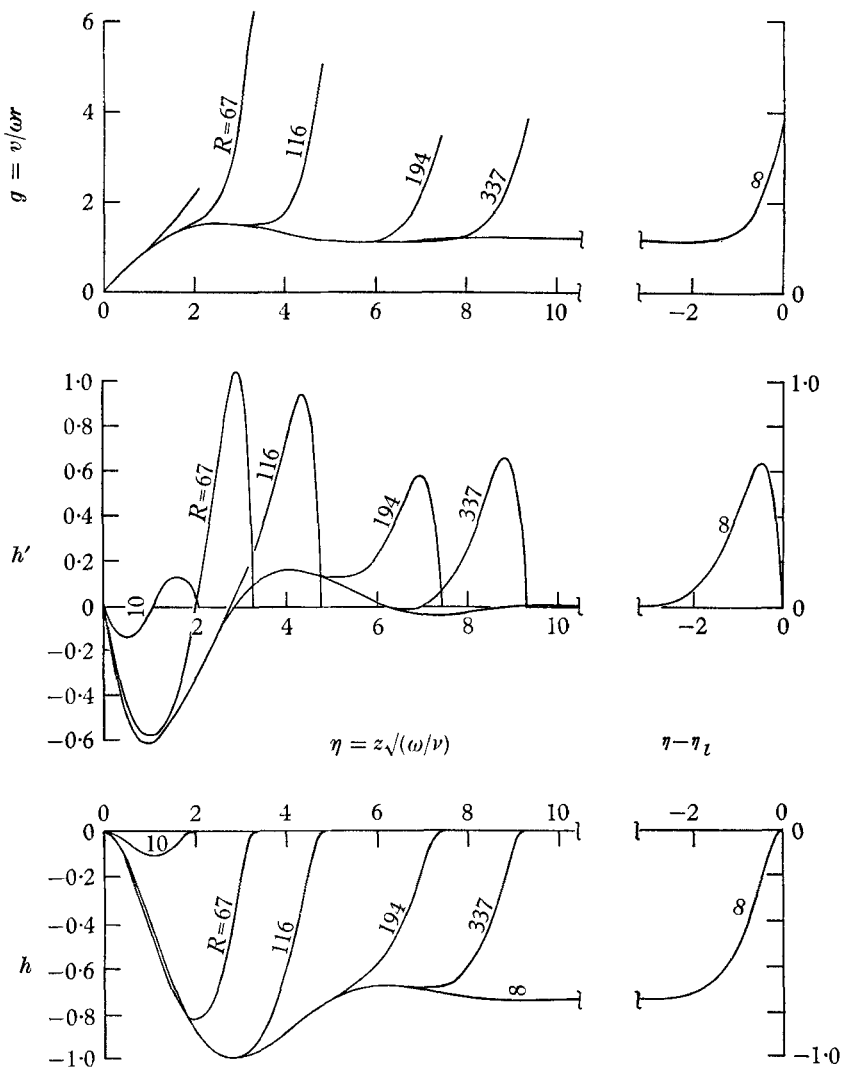

FIGURE 4. The solutions for $R = 0$ to $R = \infty$. The later limit solution corresponds to a solid rotational core bounded by layers with circumferential velocities of the same sense. The Bödewadt solution is also contained in this plot.

asymptotic expansions' reported by Van Dyke (1964). This rather formal analysis has been confined to the appendix so that we can here describe the principal results in simple terms. The outer flow is defined as the flow between the stationary disk and the thin boundary layer on the rotating disk. For small enough $(\Omega l^2/\nu)^{-\frac{1}{2}}$ we find that the circumferential velocity is essentially zero as

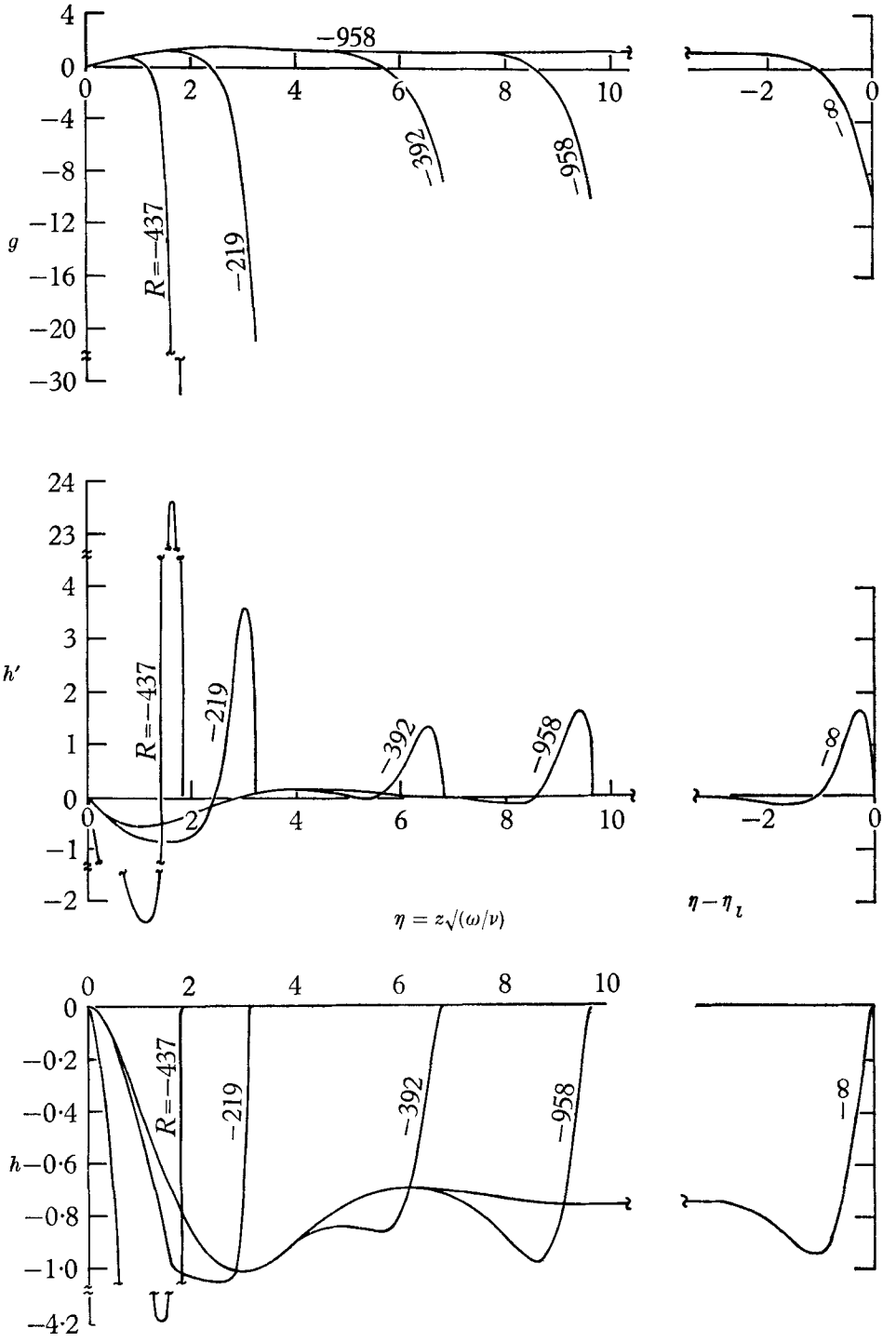

FIGURE 5. The solutions for $R = -\infty$ to finite values. Circumferential velocities on the boundaries are in the opposite sense. The Bödewadt solution is also contained in this plot.

compared to the large circumferential velocity in the boundary layer which is given by the von Kármán solution. The main function of the outer flow is to supply axial flow to the inner boundary-layer flow, which is then centrifuged outward. The first-order solution of the outer flow is, in fact, given by

$$v = 0, \tag{24a}$$

$$u = -0{\cdot}886(\Omega\nu)^{\frac{1}{2}}(r/l)\,\xi, \tag{24b}$$

$$w = 0{\cdot}886(\Omega\nu)^{\frac{1}{2}}\xi^2. \tag{24c}$$

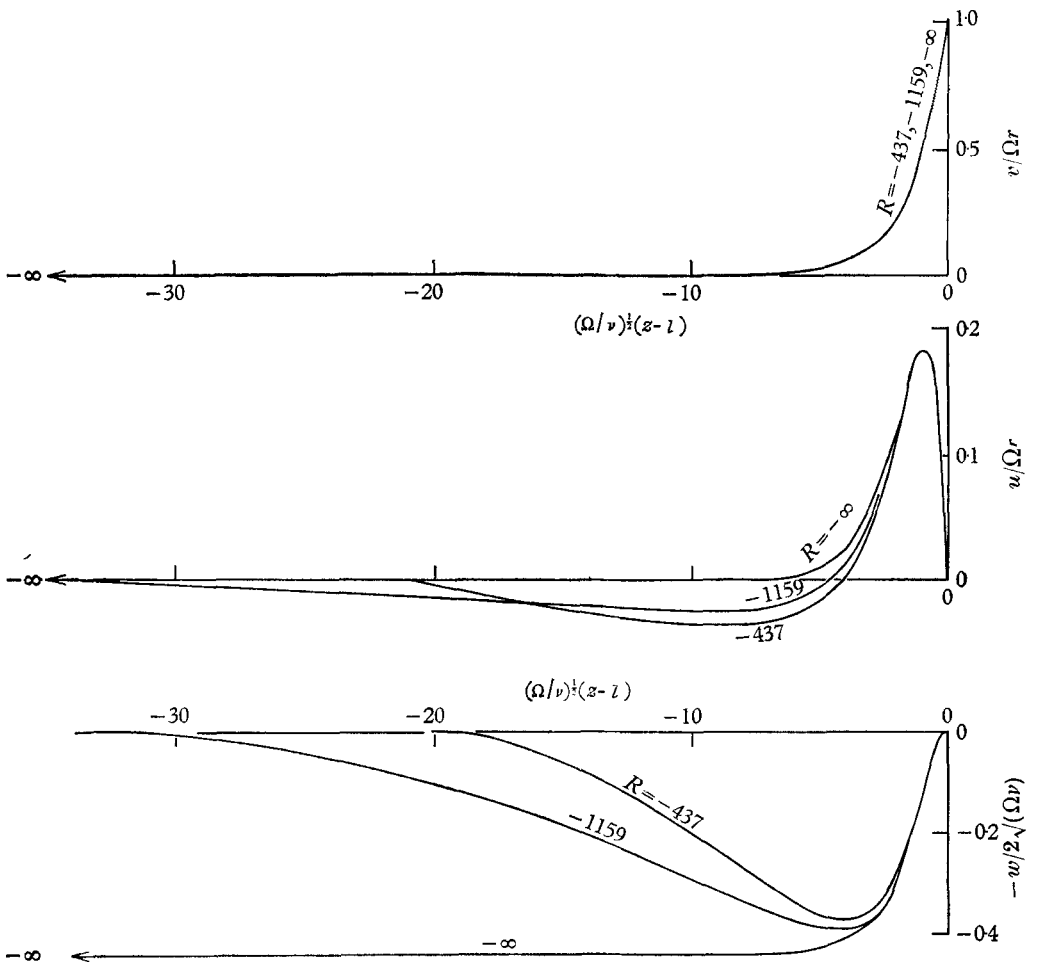

FIGURE 6. A continuation of the solutions of figure 5 from R equal to finite values to $R = -\infty$ again. The variables have been rescaled, however, so that the von Kármán limiting solution remains finite. Note that the solutions for v do not exactly overlap but the differences are very small.

At $\xi = 1{\cdot}0$, $w = 0{\cdot}886(\Omega\nu)^{\frac{1}{2}}$ is just the axial velocity required by the free-disk flow. Equations (24*a–c*) represent a vorticity-preserving flow or more precisely $\omega(z,r) = (\partial u/\partial z - \partial w/\partial r) \propto r$, which accounts for the shrinking of vortex tubes while fluid moves radially inward. It can now be verified that equations (24*a–c*) are, in fact, exact solutions to equations (1)–(4). Actually, they were

first obtained by Stewartson (1953); the appendix merely provides a systematic means of finding higher-order corrections.

We have, by the way, recomputed the free-disk flow using starting values provided by equations (23*a*, *b*), where now $g_0 = 0$. We find that our solution agrees in the third decimal place with the results reported by Cochran (1934).

4. Experimental results

A small apparatus was constructed consisting of a rotating and stationary disk, 4·29 in. radius and separated by an axial clearance of $\frac{1}{8}$ in. The rotating disk was run at speeds to give $R = \Omega l^2/\nu = 50$ and 100; at standard atmospheric conditions this corresponds to $\Omega = 730$ and 1460 rev/min.

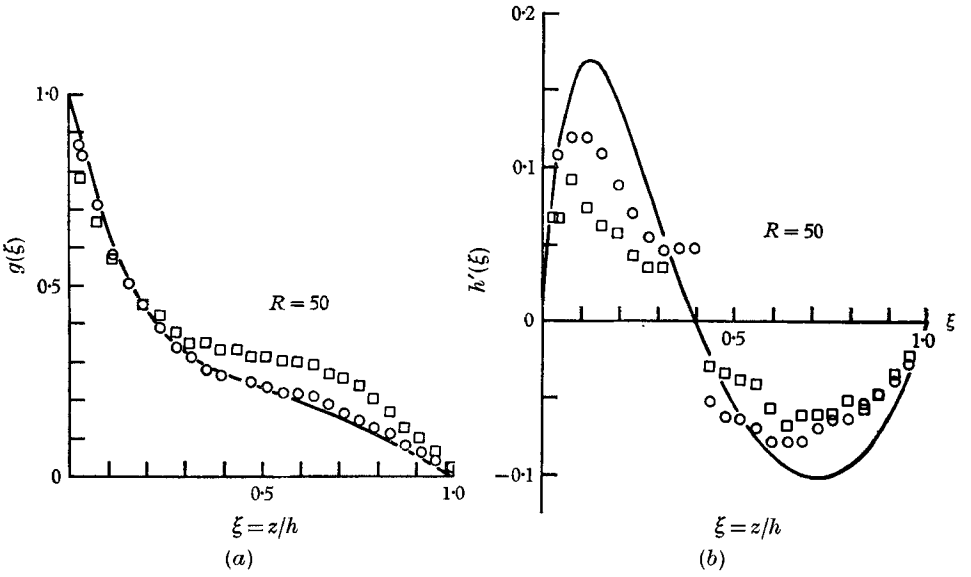

FIGURE 7. Hot-wire velocity measurements compared with calculations at $R = 50$. The disk spacing was $\frac{1}{8}$ in., radius 4·29 in., and the rotational speed was 730 rev/min. ○, measurements at 1·77 in. radius; □, 3 in. radius.

A constant-current, hot-wire anemometer which was frequently recalibrated was used to measure the tangential velocity, and the radial velocity. Further, details of the apparatus and an estimate of errors are contained in the report by Chapple & Stokes (1962).

When the apparatus was initially run, the flow became turbulent at a Reynolds number $\Omega l^2/\nu \simeq 70$. Correspondingly the Reynolds number based on outer radius, $\Omega r_0^2/\nu$, was 45,000, which is one-tenth the transition value of a free disk as found by Gregory, Stewart & Walker (1955). Hot-wire probing indicated the source of the turbulence to be in the outward-flowing air at the outer juncture of the rotating disk and a stationary hardboard sheet which was flush with the disk. This turbulent air was then re-ingested on the stationary-disk side of the apparatus. The clearance between the disk and the hardboard sheet was then increased slightly, and suction was applied without result.

Finally the hardboard sheet was removed, leaving free edges, and the edges of both disks were machined to a $\frac{3}{16}$ in. radius. The flow was then free of turbulence for R = 100 and less.

Circumferential and meridional velocity measurements are shown in figures 7*a*, *b* and 8*a*, *b* for $R = 50$ and 100 respectively. Measurements were made at radii of 1·77 and 3·0 in. The data shown are the average of two sets taken at different times. The differences in the two sets were in all cases negligibly small. The theoretical predictions shown in the figures correspond to the first, one-cell branch of solutions.

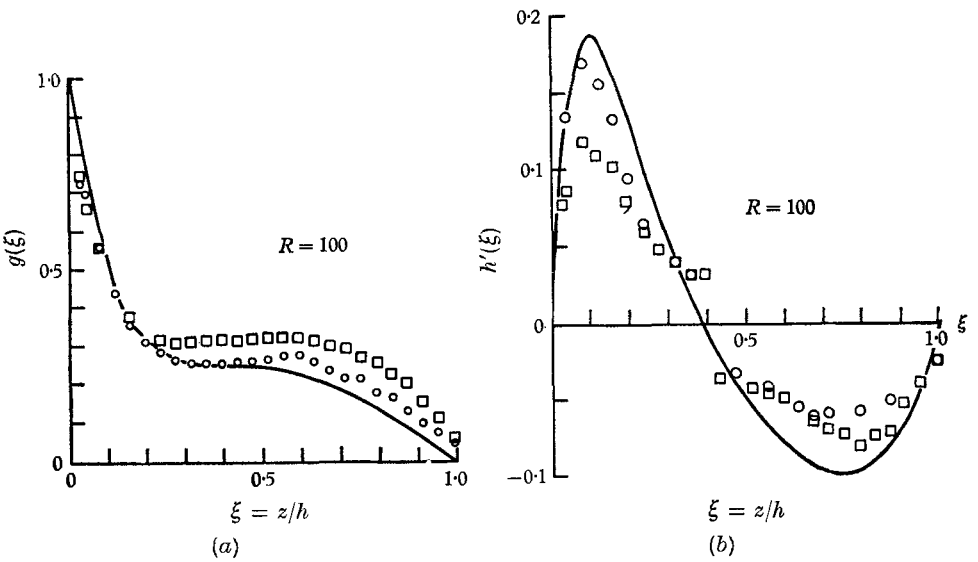

FIGURE 8. Hot-wire velocity measurements compared with calculations at $R = 100$. The rotational speed was 1460 rev/min. ○, 1·77 in. radius; □, 3 in. radius.

In the case of the inner-radius measurements of the circumferential velocity, agreement between theory and data is quite good, although there are some obvious errors near the disk surfaces. It is probable that the outer radius measurements are just as reliable and that, there, the difference between theory and data is due to the fact that the disks have a finite radius.

Comparison of the radial velocities is less satisfactory and is partly explained by the fact that the radial velocities are quite a bit smaller than the circumferential velocities. Actually, the hot wire measures the total meridional velocity component

$$\left(\frac{u^2+w^2}{\Omega^2 r^2}\right)^{\frac{1}{2}} = \left(H'^2 + 2\frac{l}{r}H^2\right)^{\frac{1}{2}},$$

but at the inner and outer radius we have $2l/r = 1{\cdot}41$ and 0·083, and H is less than 0·05 for both Reynolds numbers; the axial velocity is therefore negligible. The non-zero radial velocity measured where it obviously changes sign is a real error in measurement and reflects the difference between the uniform flow in which the wire was calibrated and the highly sheared flow in the apparatus. With this in mind one suspects that the radial velocities at the

inner radius are actually closer to the theoretical values than is indicated by the graphs.

In addition to the velocity measurements, the radial pressure gradient was measured. A micromanometer was used to measure pressure differentials between two different intervals of radii. In figure 9, the experimental points at $R = 100$ and only the solid points at $R = 50$ correspond to a spacing of $\frac{1}{8}$ in. and a speed of 730 and 1460 rev/min; for all the open points the rotating

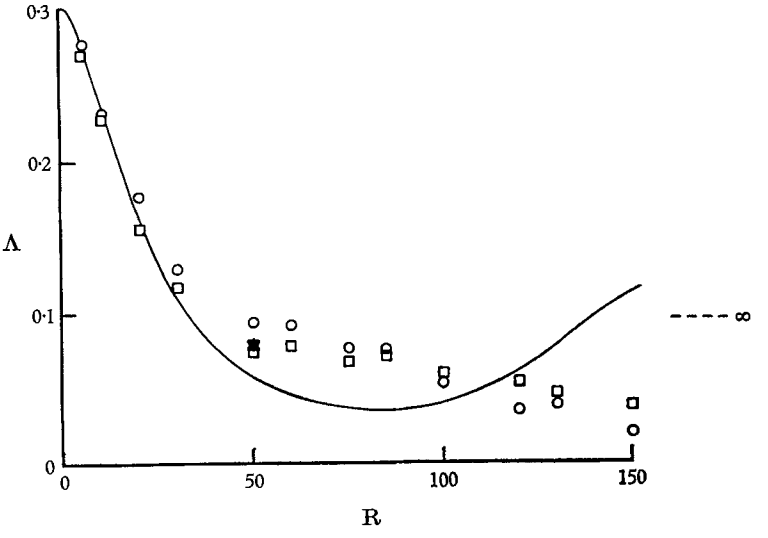

FIGURE 9. Radial-pressure-gradient measurements compared with calculated values. All of the open points correspond to 1460 rev/min while the Reynolds number was varied by varying the spacing. The solid points at $R = 50$ correspond to the conditions of figure 7. Values of Λ are obtained from table 2 ($\Lambda = h'''(0)/g^2(\eta_l)$). As $R \to \infty$, $\Lambda \to 0{\cdot}102$. □, measured between radii 1·77 and 2·375 in.; ○, measured between radii 2·375 and 3 in.

disk was maintained at the maximum rotational speed of 1460 rev/min, while the spacing was adjusted to vary the Reynolds number. This was done to maintain a measurable pressure difference level for very small Reynolds numbers. The sum of the pressure differences at the two intervals of radii agreed well with the independent measurement of the total difference across the total radial interval.

In general it is clear that the measurements are in fair agreement with the first, one-cell branch of solution. Agreement is improved for the smallest radii as expected and for the smaller Reynolds numbers. It is also clear from the measurements that the fluid near the stationary disk has been re-ingested in the apparatus and originally was the fluid near the rotating disk. The fluid therefore has a higher tangential velocity at the larger radius. It therefore seems clear that differences between theory and data are directly related to edge effects.

5. Conclusions

It is now apparent that many solutions exist for a given Reynolds number, $\Omega l^2/\nu$. We have singled out the one-cell branch solutions for detailed study and have found two sub-branches. The first starts at zero Reynolds number and limits to an infinite-Reynolds-number flow characterized by solid-body rotation of the core and bounded by two boundary layers on the stationary and rotating disks: the second starts with an infinite absolute Reynolds number, decreases to a minimum and then increases to infinite Reynolds number again. The latter limiting case is the free-disk solution of von Kármán characterized by a single boundary layer on the rotating disk. The limiting-flow solution between the boundary layer and the stationary disk is a rather simple solution to the Navier–Stokes equations.

The experimental data obtained for $\Omega l^2/\nu = 50$ and 100 clearly conform to the first one-cell branch of solutions. Agreement with theory improves as the radius decreases.

When the experiments were run, the second one-cell branch of solutions were unknown. It is therefore left to speculation as to the extent to which this type of flow can be realized in the laboratory. Our calculations indicate that the Reynolds number must be greater than about 220. Moreover, it is probable that edge effects are important; that is, if angular momentum produced in the boundary of the rotating disk is re-ingested at the outer radius, it is possible that the first sub-branch would still be obtained. On the other hand, if it could be arranged that the ingested air have negative (compared to the rotating disk) angular moment, then it is possible that the second one-cell flow might be obtained. But, for very large Reynolds number, it is also possible that the second one-cell flow could be obtained approximately so long as the ingested air has a small enough positive angular momentum; this is inferred from the fact that the first-order asymptotic solution for large Reynolds numbers yields zero angular velocity outside of the rotating-disk boundary layer. Also, experimental data do exist for the free-disk limit (Gregory *et al.* 1955).

Appendix

In this appendix we will examine the asymptotic solution which in the limit becomes the free-disk solution of von Kármán (1921). It is convenient to reverse the co-ordinate system so that now $z = 0$ corresponds to the rotating disk and $z = l$ is the stationary disk. If we set $\epsilon = (\Omega l^2/\nu)^{-\frac{1}{2}}$, the inner solution, near the rotating disk, can be assumed to be

$$v = \Omega r\{g_0(\eta) + \epsilon g_1(\eta) + \ldots\}, \tag{25a}$$

$$w = -2(\Omega\nu)^{\frac{1}{2}}\{h_0(\eta) + \epsilon h_1(\eta) + \ldots\}, \tag{26a}$$

$$u = \Omega r\{h_0'(\eta) + \epsilon h_1'(\eta) + \ldots\}, \tag{27a}$$

$$p/\rho = \Omega\nu\{\hat{P}_0(\eta) + \epsilon\hat{P}_1(\eta) + \ldots\} + \tfrac{1}{2}\Omega^2 r^2\{\epsilon\lambda_1 + \epsilon^2\lambda_2 + \ldots\}, \tag{28a}$$

$$\eta = z(\Omega/\nu)^{\frac{1}{2}}. \tag{29a}$$

The outer solution will be assumed to be:

$$v = \Omega r\{\epsilon G_1(\xi) + \epsilon^2 G_2(\xi) + \ldots\}, \tag{25b}$$

$$w = -2\Omega l\{\epsilon H_1(\xi) + \epsilon^2 H_2(\xi) + \ldots\}, \tag{26b}$$

$$u = \Omega r\{\epsilon H_1'(\xi) + \epsilon^2 H_2'(\xi) + \ldots\}, \tag{27b}$$

$$p/\rho = \Omega^2 l^2\{\epsilon P_1(\xi) + \epsilon^2 P_2(\xi) + \ldots\} + \tfrac{1}{2}\Omega^2 r^2\{\epsilon\Lambda_1 + \epsilon^2\Lambda_2 + \ldots\}, \tag{28b}$$

$$\xi = z/l. \tag{29b}$$

The procedure is now as follows:

(i) Insert equations (25*a*)–(28*a*) into equations (2) and (3) and collect terms of order $\epsilon^0, \epsilon^1, \ldots$. (We will here not consider the solution for the z dependence of p.).

(ii) Insert (25*b*)–(28*b*) into (2) and (3) and collect terms of order $\epsilon^0, \epsilon^1, \ldots$. Actually there are no terms of order ϵ^0. The terms of ϵ^1 yield $\Lambda_1 = 0$.

(iii) satisfy the boundary conditions at $\eta = 0$ and $\eta = 1$.

(iv) match the velocity components and the pressure near the disk, but outside the disk boundary layer. To demonstrate the matching procedure, we consider $v(\eta) = v(\xi)$ where $\xi = \epsilon\eta$. Therefore

$$\begin{aligned}\epsilon G_1(\xi)\} + \epsilon^2\{G_2(\xi)\} + \ldots &= \epsilon\{G_1(0) + \epsilon\eta G_1'(0) + \ldots\} \\ &\quad + \epsilon^2\{G_2(0) + \epsilon\eta G_2'(0) + \ldots\} \\ &\quad + \ldots \\ &= g_0(\eta) + \epsilon g_1(\eta) + \ldots.\end{aligned}$$

Collecting terms and letting $\epsilon \to 0$ we have

$$g_0(\eta \to \infty) \sim 0, \quad g_1(\eta \to \infty) \sim G_1(0), \quad \text{etc.}$$

Matching the pressures yields $\lambda_0 = 0$.

We shall now list the equations together with their corresponding boundary conditions in the order in which they must be solved:

$$\left.\begin{aligned} &h_0''' + 2h_0 h'' - h_0'^2 = -g_0^2, \\ &g_0'' + 2h_0 g_0' - 2h_0' g_0 = 0, \\ &g_0(0) = 1, \quad g_0(\eta \to \infty) \sim 0, \\ &h_0'(0) = 0, \quad h_0'(\eta \to \infty) \sim 0, \\ &h_0(0) = 0. \end{aligned}\right\} \tag{30}$$

(It should be noted that in the original set of equations λ (or Λ) was undetermined and, therefore, a third, outer-boundary condition, $h_0(\eta \to \infty)$, was required. However, $\lambda_0 = 0$ and the above equations lead to the von Kármán solution, where now a result is $h_0(\infty) = 0{\cdot}443$.)

$$\left.\begin{aligned} &2H_1 H_1'' - H_1'^2 = \Lambda_2 - G_1^2, \\ &H_1 G_1' - H_1' G_1 = 0, \\ &H_1'(1) = 0, \\ &H_1(0) = h_0(\infty) = 0{\cdot}443, \quad H_1(1) = 0, \\ &\qquad\qquad\qquad\qquad G_1(1) = 0. \end{aligned}\right\} \tag{31}$$

(In this equation set we have lost the highest-order derivative; i.e. the equations are inviscid. The differential equations are third order but Λ_2 is arbitrary.)

$$\left.\begin{aligned} &h_1''' + 2h_0h_1'' - 2h_0'h_1' + 2h_0''h_1 = -2g_0g_1, \\ &g_1'' + 2h_0g_1' + 2h_0'g_1 = 2g_0h_1' - 2h_1g_0', \\ &g_1(0) = 0, \quad g_1(\eta \to \infty) \sim G_1(0), \\ &h_1'(0) = 0, \quad h_1'(\eta \to \infty) \sim H_1'(0), \\ &h_1(0) = 0. \end{aligned}\right\} \tag{32}$$

Equations (30) yield the von Kármán solution, which calls for an axial velocity flow to the disk boundary layer. This axial flow is essentially supplied by the solution to equations (31).

The solution to equations (31) is remarkably simple. If we set $\Lambda_2 = 0$ it is possible to satisfy the differential equations and all of the boundary conditions with

$$\left.\begin{aligned} G_1 &= 0, \\ H_1 &= 0{\cdot}443(1-\xi)^2. \end{aligned}\right\} \tag{33}$$

REFERENCES

BATCHELOR, G. K. 1951 Note on a class of solutions of the Navier–Stokes equations representing steady rotationally symmetric flow. *Quart. J. Mech. Appl. Math.* **4**, 29.

BÖDEWADT, U. T. 1940 Die Drehströmung über festem Grunde. *ZAMM* **20**, 241.

CHAPPLE, P. J. & STOKES, V. K. 1962 On the flow between a rotating and a stationary disk. *Report FLD* no. 8, Dept. of Mech. Engng, Princeton University.

COCHRAN, W. G. 1934 The flow due to a rotating disk. *Proc. Camb. Phil. Soc.* **30**, 365.

GREGORY, N., STEWART, J. T. & WALKER, W. S. 1955 On the stability of three-dimensional boundary layers with application to the flow due to a rotating disk. *Phil. Trans.* A **248**, 155.

GROHNE, D. 1955 Über die laminar Strömung in einer kreiszylindrischen Dose mit rotierendem Deckel. *Nachr. Akad. Wiss. Göttingen*, **12**, 263.

LANCE, G. N. & ROGERS, M. H. 1962 The axially symmetric flow of a viscous fluid between two infinite rotating disks. *Proc. Roy. Soc.* A **266**, 109.

PEARSON, C. E. 1965 Numerical solutions for the time-dependent viscous flow between two rotating coaxial disks. *J. Fluid Mech.* **21**, 623.

ROGERS, M. H. & LANCE, G. N. 1960 The rotationally symmetric flow of a viscous fluid in the presence of an infinite rotating disk. *J. Fluid Mech.* **7**, 617.

STEWARTSON, K. 1953 On the flow between two rotating coaxial disks. *Proc. Camb. Phil. Soc.* **49**, 333.

VAN DYKE, M. 1964 *Perturbation Methods in Fluid Mechanics*. New York: Academic Press.

VON KÁRMÁN, T. 1921 Laminar und turbulente Reibung. *ZAMM* **1**, 233.